Inducing Aromaticity Patterns and Tuning the Electronic Transport of Zigzag Graphene Nanoribbons via Edge Design

ARTICLE *in* THE JOURNAL OF PHYSICAL CHEMISTRY C · NOVEMBER 2013

Impact Factor: 4.77 · DOI: 10.1021/jp410032h

THE JOURNAL OF PHYSICAL CHEMISTRY C

Article

pubs.acs.org/JPCC

Inducing Aromaticity Patterns and Tuning the Electronic Transport of Zigzag Graphene Nanoribbons via Edge Design

Francisco J. Martín-Martínez,* Stijn Fias, Balázs Hajgató, Gregory Van Lier, Frank De Proft, and Paul Geerlings.

Research Group of General Chemistry (ALGC), Vrije Universiteit Brussel (VUB), Pleinlaan 2, 1050 Brussels, Belgium

ABSTRACT: Despite its remarkable electronic properties, graphene is a semimetal, or zero-band-gap semiconductor, which limits its potential applications in electronics. Cutting graphene into nanoribbons is one of the most successful approaches to opening the band gap of graphene toward applications. However, whereas armchair graphene nanoribbons exhibit semiconducting behavior, zigzag-edged structures are still semimetals. In this work, we perform periodic density functional theory (DFT) calculations on the electronic structure, together with nonequilibrium Green's function (NEGF) transport-property calculations, of different tailored-edge zigzag graphene nanoribbons. More precisely, we provide a complete description of the relation between band gap, transport properties, and aromaticity distribution along these materials, based on DFT results and Clar's sextet theory. The edge design is also shown to be applicable for finite fragments of carbon nanotubes in which the electronic confinement is similar. This ansatz provides different methods for the rational edge design of zigzag graphene nanoribbons, which induces aromaticity patterns and opens the band gap toward electronic applications. The mean bond length (MBL) geometric parameter and the six-center index (SCI) aromaticity descriptor are used to analyze the aromaticity patterns.

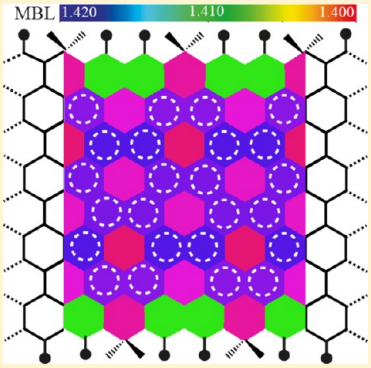

INTRODUCTION

In the race to develop post-silicon electronic devices based on carbon nanomaterials, graphene has arisen as the leading candidate.[1] Its outstanding electronic properties have propelled great research efforts to develop novel carbon-based materials for electronic applications.[2,3] However, bidimensional graphene presents an intrinsic characteristic that hampers many of its potential applications in electronics, as it is a semimetal and, therefore, it does not have an adequate energy band gap for electronic applications. Nevertheless, new successful approaches have been put forward to open the band gap of graphene, and one of the most remarkable is the cutting of graphene into graphene nanoribbons (GNRs).[4] GNRs are tailored narrow strips of graphene whose structural and electronic properties exhibit a combination of surface and edge characteristics. In fact, quantum confinement and edge effects render narrow GNRs semiconducting.[5] To achieve sufficient on/off ratios in semiconducting devices, lateral dimensions of less than 10 nm are required, and only widths of less than 3 nm provide a band gap that falls in the same range of the current worldwide-used semiconductor materials. One of the great advantages of GNRs over other similar nanomaterials such as carbon nanotubes (CNTs)[6] is that they can be patterned with atomic precision using chemical,[7,8] sonochemical,[9] and lithography[10] methods, and therefore, reliable production of GNRs narrower than 10 nm should be achievable, although it is still a significant challenge. Even more, because only 20-nm widths can be reached so far with experimental techniques,[11] theoretical predictions are needed to study the rational design of widths and edge geometries for these strips of carbon. This is of major importance because, although GNRs present versatile electronic and magnetic properties,[12−14] not all GNRs are the same, and the electronic properties are very sensitive to the geometry of the edges and the width of the ribbon.[15−17] In this respect, it is important to distinguish between zigzag and armchair GNRs. Armchair GNRs have been shown to present desirable band gaps, whereas zigzag GNRs seem to remain semimetallic despite confinement in one direction. Additionally, the existence of a nonzero band gap is closely related to the aromaticity distribution and electronic delocalization along these structures,[18] and therefore, the study of these chemical properties is crucial for predicting the electronic properties of these materials.[19] In recent studies, the close relation between the existence of so-called aromaticity patterns and the band gap has been extensively demonstrated.[18,20] Armchair GNRs (those with nonzero band gaps) present such aromaticity patterns (see the right side of Figure 1) where aromatic rings are arranged along the graphitic structure in any of three types of patterns already described extensively in literature,[21,22] namely, Clar, Kekulé, and incomplete-Clar patterns. On the contrary, zigzag GNRs are uniform structures in which all of the rings are almost equivalent (see the left side of Figure 1) and have similar aromaticity values and no pattern is present. The fact that aromaticity patterns are closely related to the existence of a band gap in GNRs makes it

Received: October 9, 2013
Revised: November 11, 2013
Published: November 14, 2013

   dx.doi.org/10.1021/jp410032h | J. Phys. Chem. C 2013, 117, 26371−26384

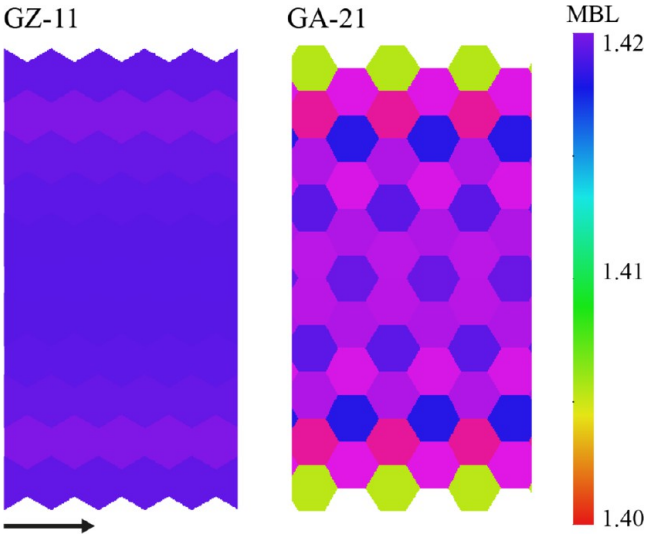

Figure 1. MBL representation of HSE06/6-31G*-optimized structures of (left) GZ-11 and (right) GA-21 GNRs.

important to control the aromaticity distribution along these materials to induce a band-gap opening. In fact, controlling the aromaticity patterns has already been shown to be a suitable method for designing redox-switchable devices based on GNRs.[23] In the present work, based on basic knowledge of Clar's sextet theory,[24,25] which has been demonstrated to be a suitable theory for nanomaterials,[18,20,26−29] we perform periodic density functional theory (DFT) calculations on the electronic structure of tailored-edge zigzag GNRs, focusing on their aromaticity patterns and the connection of these patterns to the band gap and transport properties. These results are compared with the analysis of carbon nanotubes (CNTs), for which the capping[30] or the edges[18,31] similarly influence the aromaticity patterns of the whole system. We also perform DFT, density functional tight-binding (DFTB), and tight-binding (TB) calculations on the electronic transport properties of the molecular junctions, calculated by a fully self-consistent nonequilibrium Green's function (NEGF).

The analysis of the aromaticity patterns, together with the Clar's sextet theory rationalization and the transport-property calculations, provides a theoretical road map for the rational edge design of GNRs toward electronic applications.

METHODOLOGY AND COMPUTATIONAL DETAILS

The Gaussian 09 package[32] was used to perform DFT calculations with periodic boundary conditions (PBCs). Optimized geometries and electronic structures for all GNRs were obtained using the 6-31G* basis set and the hybrid Heyd−Scuseria−Ernzerhof functional (HSE06),[33] which has been demonstrated to provide accurate predictions of the electronic properties of low-dimensional graphene derivatives.[34] In all calculations, spin-restricted wave functions and a singlet ground state were considered. Some studies have suggested that the ground state for some of these systems could have an open-shell multiradical character,[35,36] but this suggestion has been put into question by other studies stating that some of these results arise from a too-limited treatment of electron correlation in DFT.[37−41] Also, changes from closed-shell to open-shell states might involve changes in the aromaticity of the rings considered.[42] Being aware of this controversy and open discussion concerning spin-restricted considerations for GNRs, we considered spin-restricted wave functions and a singlet ground state throughout this work.

For analysis of the geometry and aromaticity of the structures under consideration, we calculated the mean bond length (MBL) geometry parameter[43] and the six-center index (SCI) aromaticity descriptor,[44] respectively. The MBL quantifies the ring size of graphitic systems and is defined as the mean length of the six bonds composing a particular ring, given by

$$\mathrm{MBL} = \bar{x} = \frac{1}{6}\sum_{i=1}^{6} x_i \tag{1}$$

in which x is the C−C bond length.

The SCI quantifies the delocalization in the six-membered rings of GNRs by integrating the six-electron exchange function over the six atomic domains of the ring. Using Mulliken atom partitioning (closed-shell), by which the SCI was originally defined, the SCI can be written as

$$\mathrm{SCI} = \frac{6}{2^5}\sum_{\nu\in A}^{K}\sum_{\mu\in B}^{K}\cdots\sum_{\xi\in F}^{K}\sum_{i}^{5!}\mathcal{P}_i[(PS)_{\nu\mu}(PS)_{\mu\lambda}...(PS)_{\psi\xi}(PS)_{\xi\nu}] \tag{2}$$

in which P is the charge and bond-order density matrix and S is the overlap matrix of the basis functions. The Greek symbols refer to the basis functions, and $\mathcal{P}_i$ is a permutation operator that generates 5! terms by interchanging the Greek basis function labels from μ to ξ. The final SCI value is relative to benzene, which represents a value of 100 on the SCI scale.

Furthermore, we used Clar's sextet theory to design the zigzag GNR's edges, and therefore, it is important to introduce some basic concepts of this theory before going further into the details of our approach. In organic chemistry, the existence of a so-called aromatic ring is usually denoted by a circle inscribed in a hexagon, which indeed represents the six delocalized π electrons arising from the conjugation of double bonds and single bonds. This is known as the "Clar sextet" or "Clar ring". When such Clar rings are located along the structure of a specific polyaromatic hydrocarbon (PAH) to elucidate its aromaticity distribution, different arrangements of these circles (Clar rings) are possible. These different arrangements of Clar rings are called Clar configurations, and their combination leads to the final structure of the molecule. According to Clar's theory, the configurations with higher numbers of Clar rings along the structure will contribute more to the final distribution of aromatic sextets. Based on these very simple concepts, this theory has traditionally been applied to PAHs, helping to elucidate the aromaticity distribution simply by drawing circles in the hexagons. Recently, this approach has also been extended to the study of nanomaterials such as CNTs and GNRs.[18−24,45] For periodic systems such as GNRs, these concepts should be applied to the unit cell.

In this work, the electronic transport properties of the molecular junctions were calculated by a fully self-consistent nonequilibrium Green's function (NEGF) formalism[46] in conjunction with the DFT, density functional tight-binding (DFTB),[47] and tight-binding (TB)[48] techniques implemented in Atomistix ToolKit (ATK) package (version 12.8.2).[49−51] In our DFT calculations of the transport properties, we used the Perdew−Burke−Ernzerhof (PBE) functional[52] in conjunction with a double-ζ basis set using a norm-conserving pseudopotential (built in ATK) with a 75-hartree mesh-cutoff value. The TB calculations were used in conjunction with the Cerdá

dx.doi.org/10.1021/jp410032h | J. Phys. Chem. C 2013, 117, 26371−26384

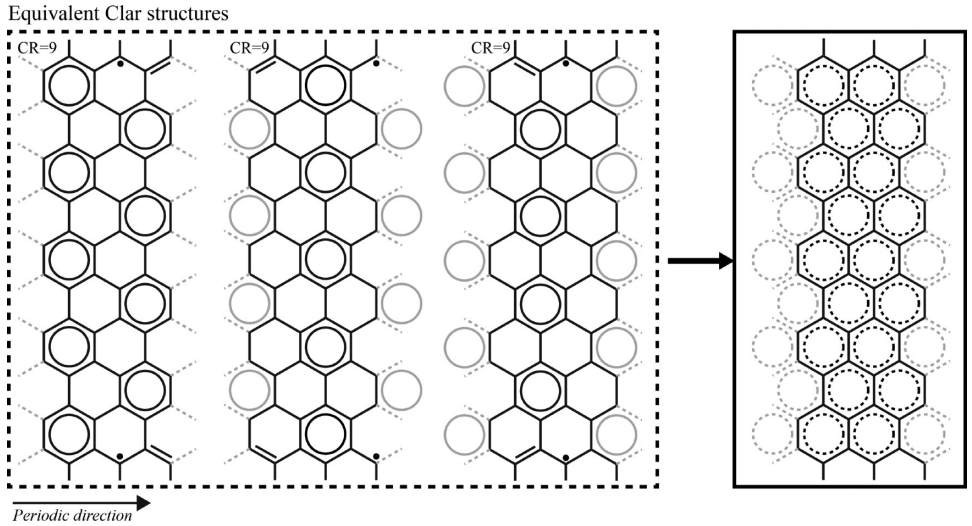

Figure 2. Three different Clar configurations for the unit cell of a GZ-9 GNR and the final structure resulting from the combination of the three. The unit cell is depicted in black, and those bonds beyond the unit cell are shown in gray. Clar rings that fall outside the unit cell are also shown in gray but with dashed lines. Unpaired electrons in the basic Clar configurations are indicated with black dots.

parameter set[53] for carbon (graphite) and hydrogen (ethylene) and the Hoffman parameter set for oxygen. DFTB calculations were performed using the MIO parameter set (ref 47, version 1.1) and the CP2K parameter set[54] for self-consistent calculations (built in ATK). All of these calculations were performed under PBCs, and the Brillouin zone was sampled with $1 \times 1 \times 100$ points within the Monkhorst−Pack k-point sampling scheme.[55] In addition, to avoid interactions between the molecule and its periodic images, a large supercell was used. For this supercell, dimensions of 25 Å in the plane perpendicular to the transport direction and parallel to the plane of the GNR and 50 Å in the plane of the GNR were used. In all transport and density-of-states (DOS) calculations, we used the DFT/HSE-optimized geometries. The left and the right electrodes were chosen to be the same with a length of approximately 7.3 Å in the transport direction, and the length of the central regions was chosen to be approximately 29.5 Å.

The notation of armchair GNRs width uses the number of dimer lines across the ribbon width, N_a, as commonly used in previous studies on this topic.[15] According to this convention, throughout this work, armchair GNRs are denoted as GA-N_a. Similarly, zigzag GNRs are denoted using the number of lines of hexagonal rings across the ribbon width, N_z, and therefore, zigzag GNRs are denoted as GZ-N_z .

RESULTS AND DISCUSSION

Zigzag GNR Edge Design. As mentioned in the Introduction, zigzag GNRs present uniform geometries in which all hexagonal rings are almost equivalent with equal size and aromaticity, whereas armchair ribbons present so-called aromaticity patterns. The fact that these patterns are closely related to the existence of a nonzero band gap in the GNR makes the control of the type of aromaticity pattern presented important for obtaining desirable transport properties. Figure 1 shows the MBL analysis of the HSE06/6-31G* fully optimized structures of two GNRs (zigzag and armchair) with approximately the same width (GZ-11 and GA-21, respectively). The zigzag GZ-11 GNR (left side of Figure 1) has a uniform color-coded MBL plot, which means that all rings present the same size and, therefore, the same aromaticity. (Recall that there is a direct relationship between aromaticity and ring size.[18,20] On the other hand, the armchair GA-21 GNR (right side of Figure 1) is patterned, with smaller rings (more aromatic) surrounded by larger rings, which is called a Clar aromaticity pattern, according to the classification already described.

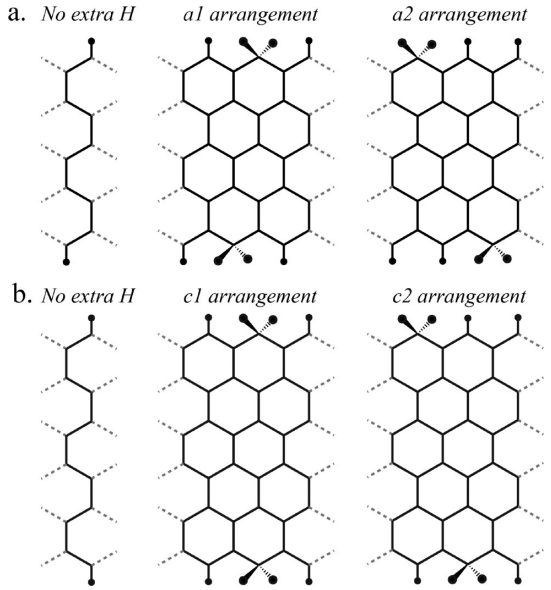

Figure 3. Four different possibilities for the one-of-three edge functionalization considered in this work for GNRs.

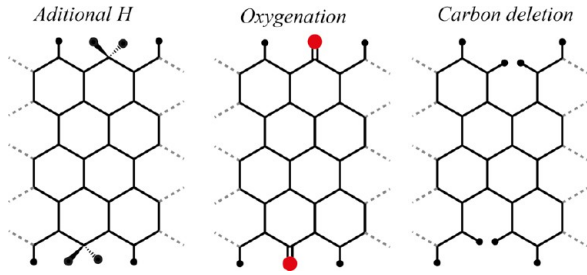

Figure 4. Three different possibilities of functionalization to induce aromaticity patterns in zigzag GNRs.

dx.doi.org/10.1021/jp410032h | J. Phys. Chem. C 2013, 117, 26371−26384

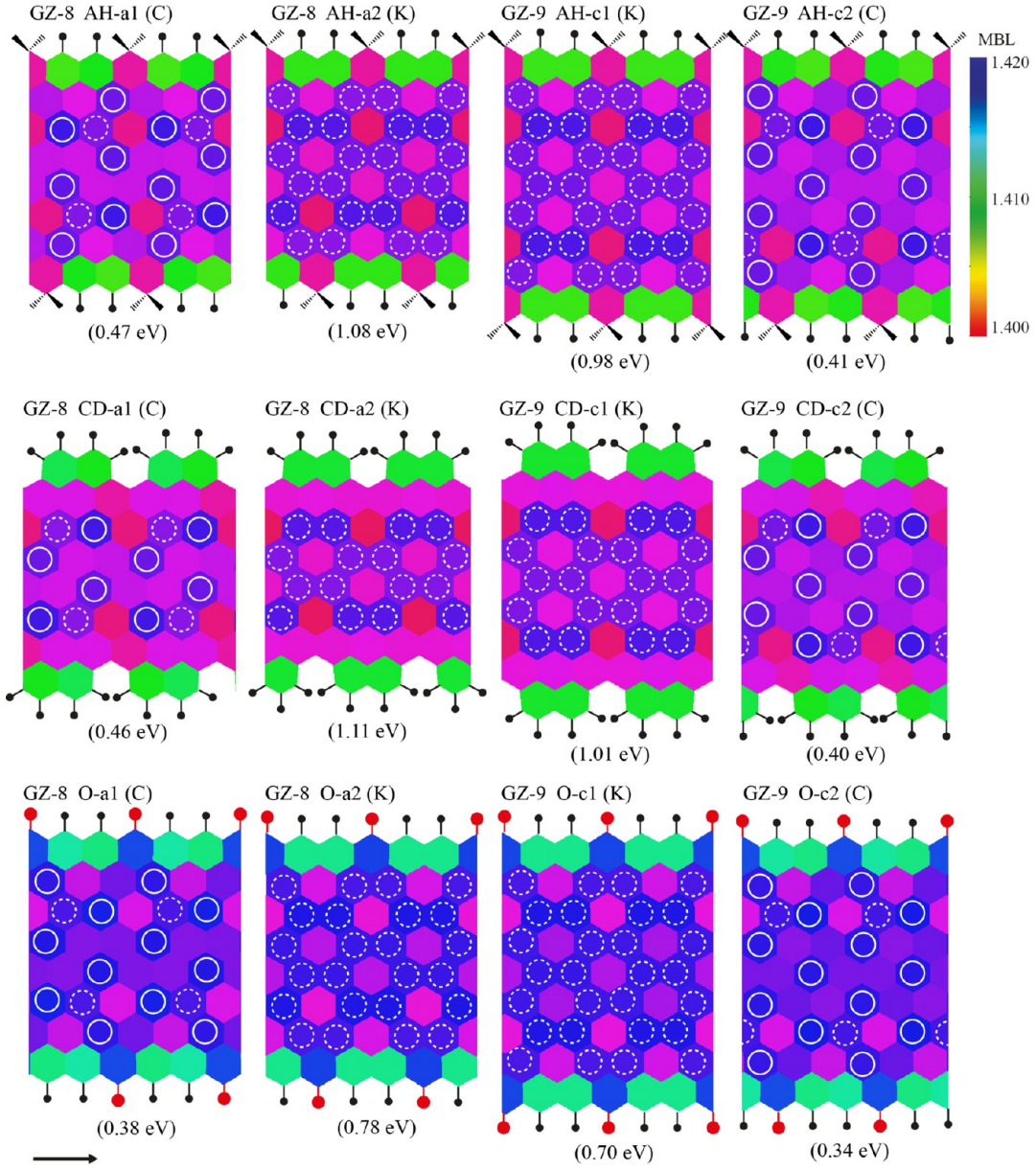

Figure 5. MBL analysis of GZ-8 and GZ-9 GNRs with AH, CD, and O functionalizations. Band-gap values are in parentheses. Geometries were optimized at the HSE06/6-31G* level of theory.

As has already been pointed out in previous articles,[16,17] the absence of these aromaticity patterns in zigzag GNRs can be explained using Clar's sextet theory.

Within this framework, Figure 2 shows the different Clar configurations for a GZ-9 zigzag GNR.

As can be noticed in Figure 2, the three possible configurations host the same number of Clar rings (CRs) per unit cell (nine rings total), and therefore, the resulting structure will be an equal combination of the three configurations (see the right side of Figure 2). The Clar rings located outside the unit cell but still at the edges contribute only partially to the total sum in the unit cell, but their contribution still has to be considered. As a consequence, all rings are equivalent, and the final structure is uniform, as observed when computing the aromaticities of the different rings. This complete delocalization of Clar sextets is depicted by dashed circles inscribed in all rings (right side of Figure 2). There is, however, an unpaired electron at the edge in all of the configurations leading to the final one (indicated by a dot in Figure 2). This issue is solved in the final structure (right side of Figure 2) through the resonance of the three Clar configurations. Therefore, there are no unpaired electrons in the zigzag GNRs but rather complete delocalization. Nevertheless, functionalizing one of three positions at the edge (e.g., with additional hydrogen) will avoid the presence of such an unpaired electron for some of the configurations, although it will also exclude the presence of a Clar sextet in the functionalized ring. Altering the edges in this way should thus lead to a different final structure, because the three possible configurations will no longer present the same numbers of Clar rings, changing their contributions to the final structure. Thus, because it alters the basic Clar configurations, this one-of-three functionalization can lead to different possibilities of aromaticity patterns, which will depend on the arrangement of the functionalized positions at the edges. In the following sections, we describe the different possibilities (two) of one-of-three functionalization that can be performed at the edge for zigzag GNRs,

dx.doi.org/10.1021/jp410032h | J. Phys. Chem. C 2013, 117, 26371−26384

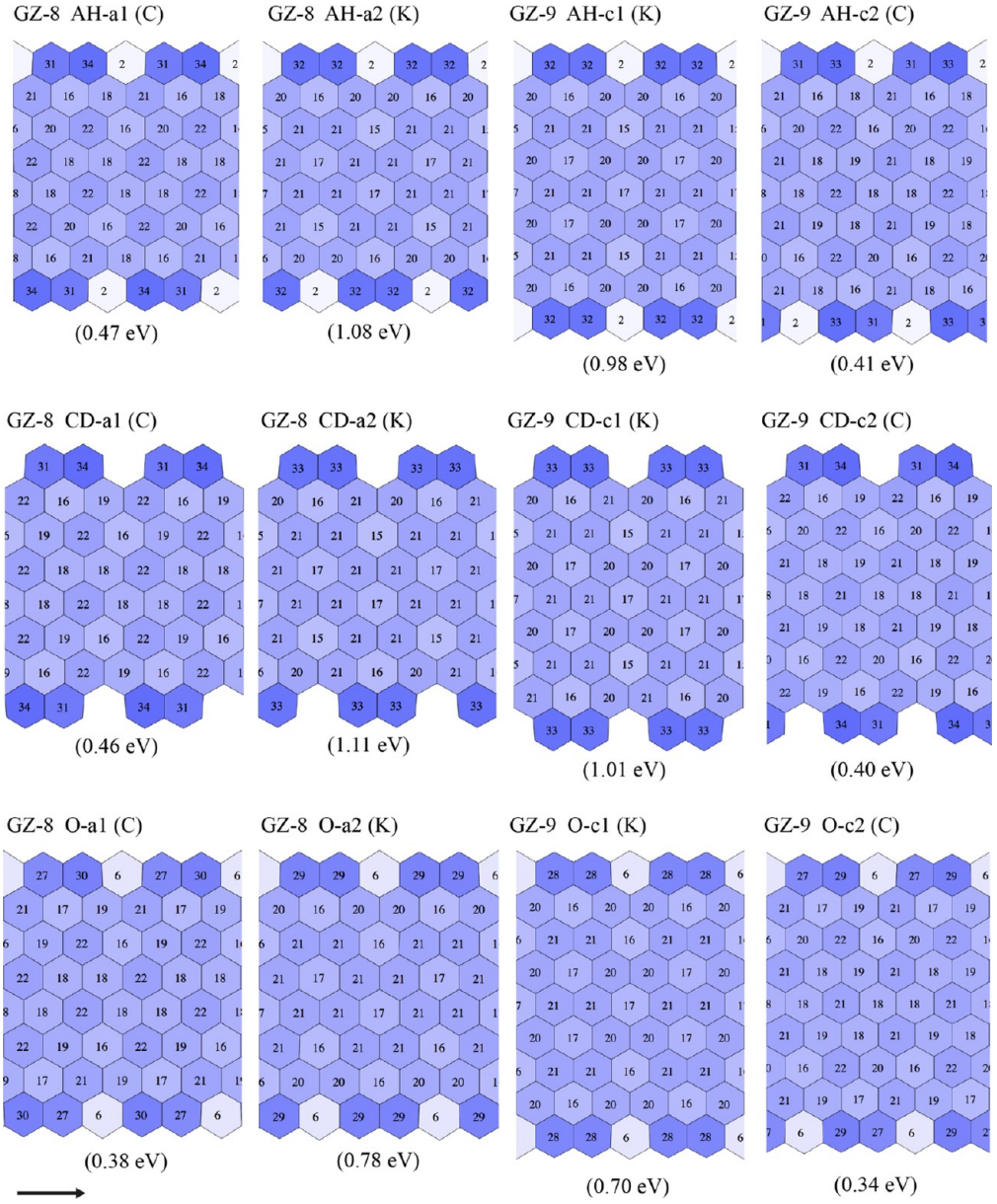

Figure 6. SCI analysis of GZ-8 and GZ-9 GNRs with AH, CD, and O functionalizations. Band-gap values are in parentheses. SCI values are indicated inside the hexagons. Geometries were optimized at the HSE06/6-31G* level of theory.

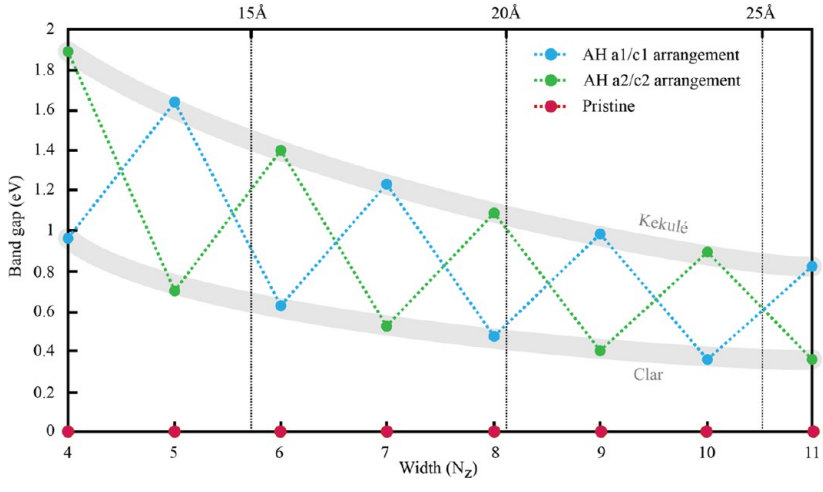

Figure 7. Band-gap values for all of the GNRs under study. Values corresponding to Kekulé, and Clar-patterned GNRs are shadowed in gray.

dx.doi.org/10.1021/jp410032h | J. Phys. Chem. C 2013, 117, 26371−26384

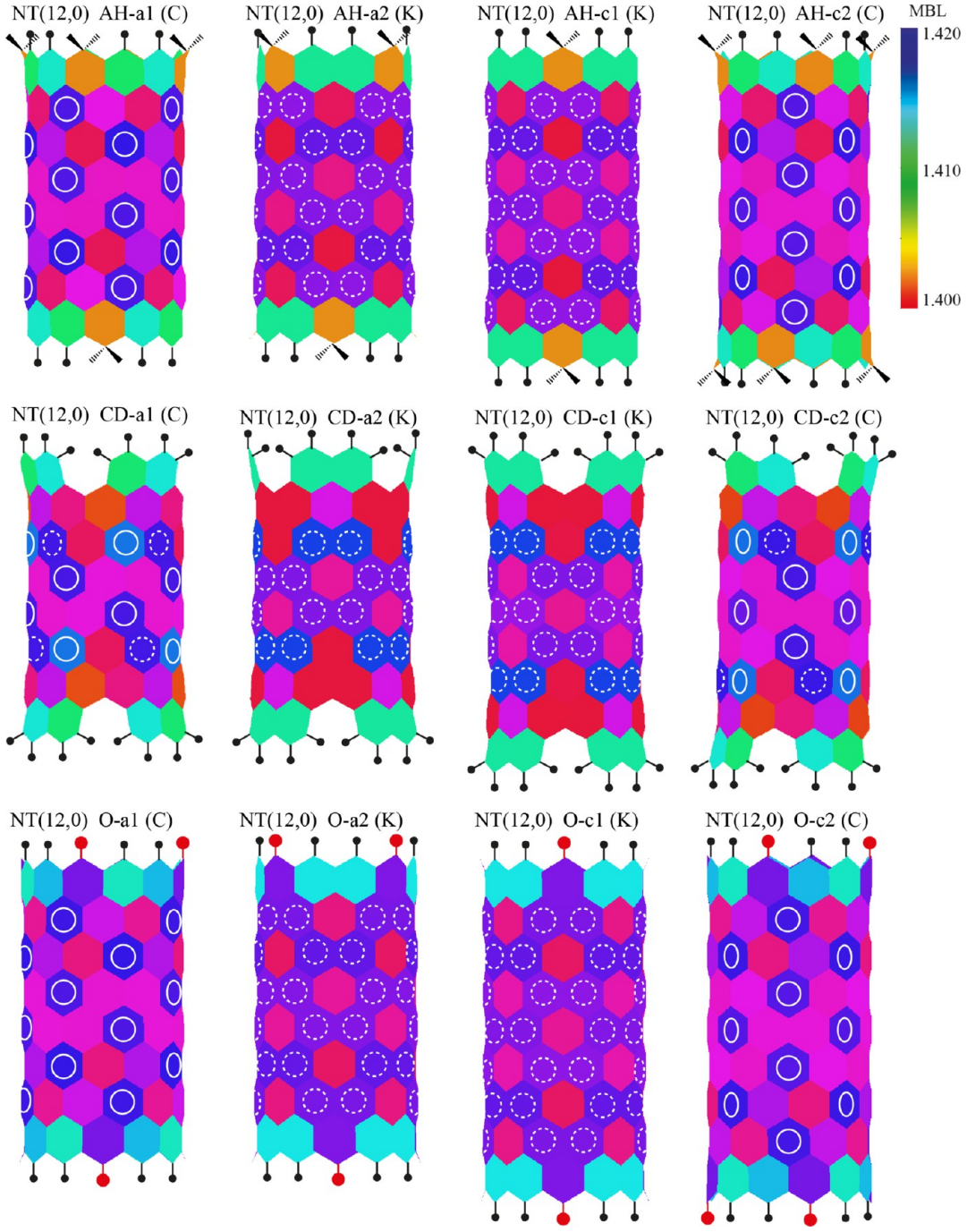

Figure 8. MBL analysis of a (12,0) CNT with AH, CD, and O functionalization. Geometries were optimized at the HSE06/6-31G* level of theory.

all of which are shown in Figure 3. All of the other possible combinations of functionalization positions (three positions on each side) are equivalent by symmetry to the studied cases.

Before explaining all of the different possibilities of one-of-three functionalization considered here, it is important to remark that there are two different types of zigzag GNRs depending on the arrangement of the terminal atoms of one edge with respect to the other: those in which the terminal atoms of one edge coincide exactly with the terminal atoms of the other edge and those in which the terminal atoms do not coincide this way but are slightly displaced. In the present article, the first type is called coincident-type (c-type) edges; this is the case when N_z is an even number (see Figure 3b). The second is called alternating-type (a-type) edges, which arise when N_z is an odd number (see Figure 3a). Hence, for each of these two types of zigzag GNRs, we performed the two different possible types of one-of-three functionalization, giving a total of four different possible structures, denoted in Figure 3a as a1 and a2 (alternating-edge GNRs) and in Figure 3b as c1 and c2 (coincident-edge GNRs).

In Figure 3, the four possibilities are exemplified with additional hydrogen atoms in the functionalized positions. This type of additional-hydrogen functionalization is indeed one of the possible ways to control the Clar structure of zigzag GNRs, but such control can also be achieved by other means. In fact, not only additional hydrogen but also any functionalization that

dx.doi.org/10.1021/jp410032h | J. Phys. Chem. C 2013, 117, 26371−26384

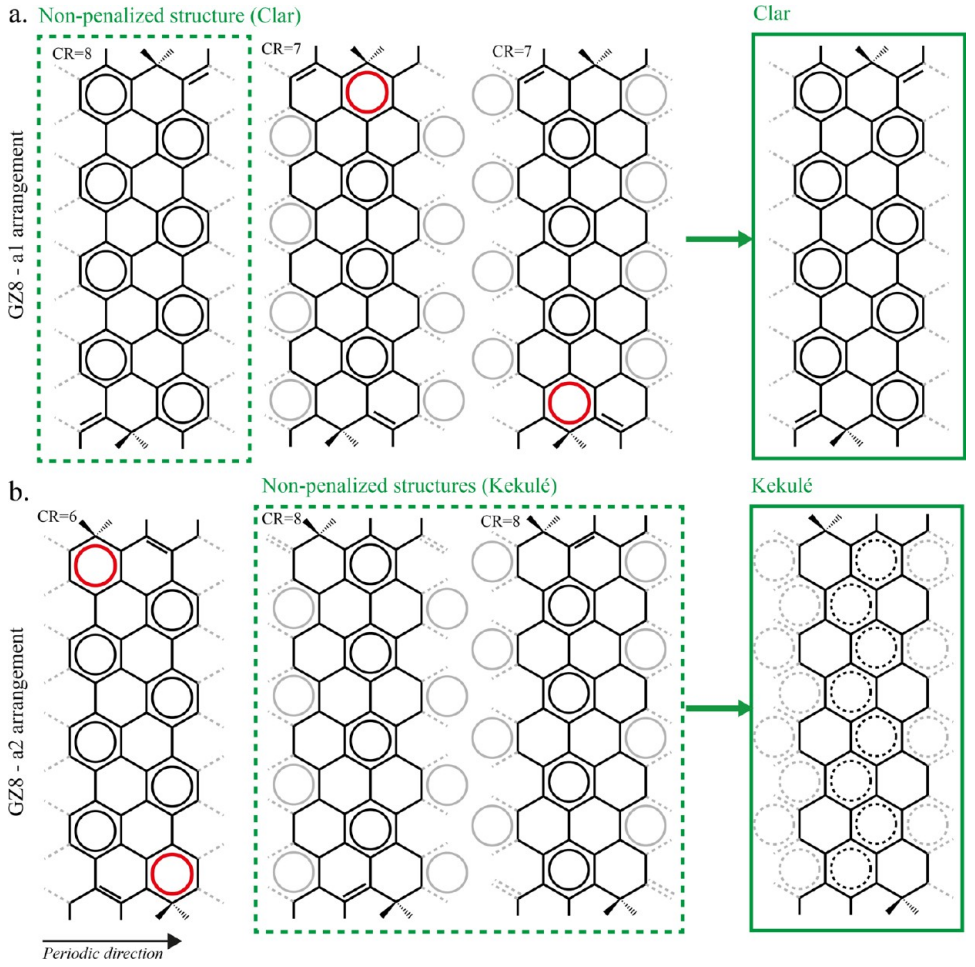

Figure 9. Representations of the three possible distributions of Clar rings along the unit cell for a GZ-8 GNR functionalized with additional hydrogen in (a) a1 and (b) a2 arrangements. Penalized Clar rings are shown in red. The final structure is highlighted in a green box (on the right).

avoids an unpaired electron in the Clar configurations and deletes the Clar sextet from this external hexagon is equally possible. For instance, addition of oxygen or even removal of the carbon atom at these positions could be useful as well. In this way, Figure 4 shows these different types of tailored edges, namely, additional hydrogen (AH), oxygen (O), and carbon deletion (CD), that avoid the unpaired electrons in the Clar configurations and delete the Clar sextet from the associated hexagon.

Induced Aromaticity Patterns and Band-Gap Opening on Zigzag GNRs. Returning to the core of the discussion, by applying this rational design to the edges of zigzag GNRs, we expected to obtain aromaticity-patterned structures similar to the patterns of armchair GNRs. In fact, as shown by our DFT calculations, zigzag GNRs with tailored edges are no longer uniform but instead present such aromaticity patterns. Figure 5 shows the MBL analysis of both GZ-8 and GZ-9 zigzag GNRs functionalized by AH, O, and CD. The aromaticity patterns are clearly seen for these tailored-edge GNRs, and more importantly, the band gaps (shown in parentheses for all of the structures) are nonzero, which changes the electronic transport properties of these structures (vide infra).

The GZ-8 GNR presents a Clar-type aromaticity pattern when an a1 arrangement is set but a Kekulé pattern when the arrangement is of type a2. This occurs for all types of functionalization (AH, O, and CD) performed on the GZ-8 ribbon. In the case of GZ-9, the situation is reversed. The c1 arrangement induces a Kekulé aromaticity pattern, whereas the c2 arrangement induces a Clar-type pattern. This opposite behavior is due to the different arrangements of terminal atoms at one edge with respect to the other edge, as will be explained later in terms of Clar's sextet theory. In both cases, GZ-8 and GZ-9, the Kekulé patterns are more pronounced than the Clar patterns. In the case of the Kekulé pattern, more-aromatic rings (denoted by dashed circles) nicely surround less-aromatic ones. However, for Clar patterns, the distribution of more-aromatic rings (denoted by circles) surrounded by less-aromatic ones, which is indeed the normal Clar-patterned arrangement, is not as clear as expected, and some partially aromatic rings appear between the most aromatic ones (denoted by dashed circles). The reasons for this will be explained later in the discussion of Clar's sextet theory. Despite this aspect, a Clar aromaticity pattern is still present in the GZ-8-a1 and GZ-9-c2 structures, in contrast to the Kekulé pattern shown by the GZ-8-a2 and GZ-9-c1 structures.

These results are also supported by the SCI calculations shown in Figure 6. In the SCI analysis, we found that the functionalization of a ring at the edge decreases the SCI value from around 30% to 2%, clearly demonstrating that both the AH and O functionalizations destroy the π aromatic system of the ring in which they are located. In these SCI plots, the Clar structures (GZ-8-a1 and GZ-9-a2) present more-aromatic rings, with SCI values around 20−22%, surrounded by less-aromatic ones, with SCI values close to 16−18%. As discussed with

dx.doi.org/10.1021/jp410032h | J. Phys. Chem. C 2013, 117, 26371−26384

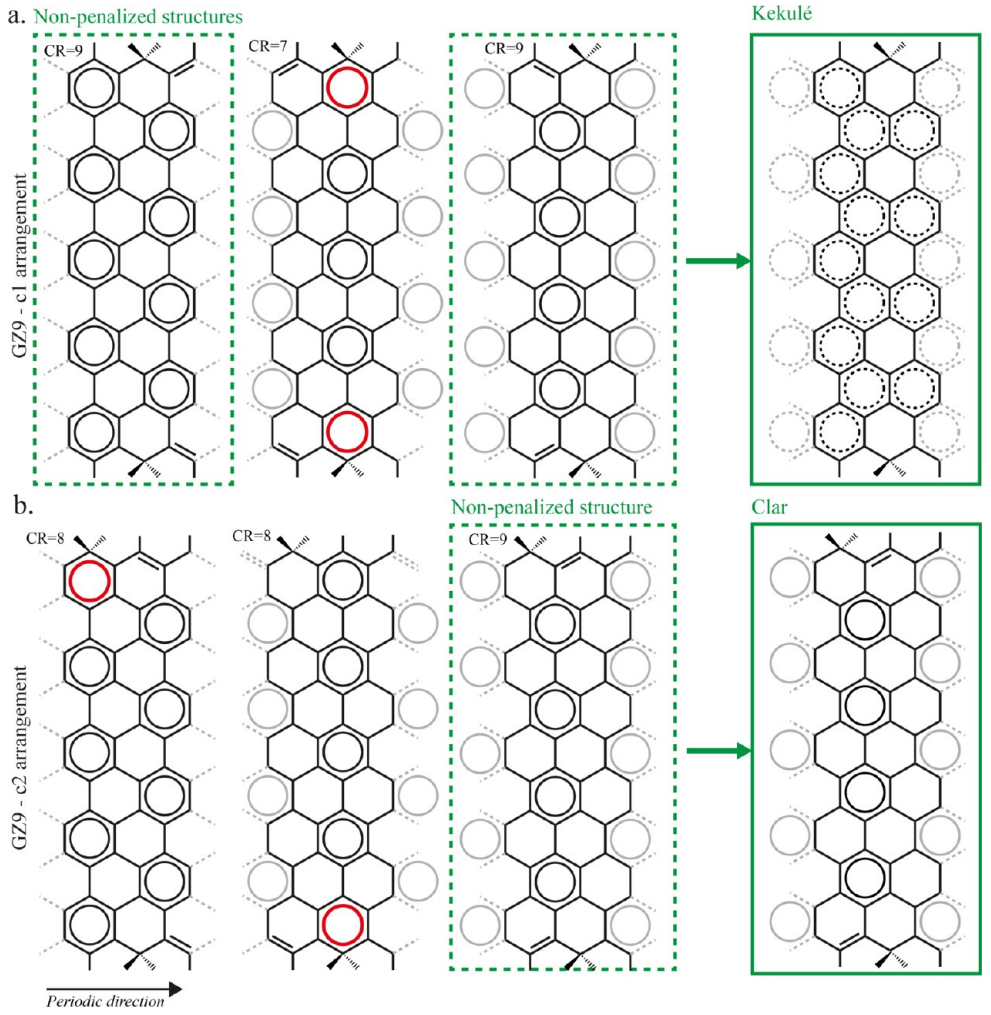

Figure 10. Representations of the three possible distributions of Clar rings along the unit cell for a GZ-9 GNR functionalized with additional hydrogen in (a) c1 and (b) c2 arrangements. Penalized Clar rings are shown in red. The final structure is highlighted in a green box (on the right).

respect to the MBL plots, however, these Clar patterns present some partially aromatic rings, with SCI values of 19% and 20%, that are between the more-aromatic (22%) and less-aromatic (16%) ones. In the case of Kekulé patterns, the arrangement is completely clear, as was the case for MBL values. For Kekulé patterns, rings with SCI values of 20% and 21% surround less-aromatic rings with values of 17%.

Concerning the band-gap values, which are displayed in Figures 5 and 6, Kekulé-patterned structures present the highest band-gap values in all cases. This also influences the electronic transport properties of the structures, as discussed later in detail. Considering the different types of functionalization, AH and CD functionalizations present similar band-gap values, whereas in O-functionalized structures, the band gap is slightly smaller within the same arrangement. This is in accordance with the range in which MBL values are displayed. AH- and CD-functionalized structures are in the same range of values for MBL, whereas for O-functionalized structures, the range is displaced.

Figure 7 brings together the band-gap values of all of the structures under study (GNRs with N_z = 4–9) for the AH functionalization, in comparison to those of the nonfunctionalized GNRs. Structures with functionalization in the a1 and c1 arrangements are depicted in green, whereas a2 and c2 arrangements are in blue. The value of the band gap as the width of the ribbon is increased for both a1/c1 and a2/c2 arrangements describes a zigzag-shaped curve, which goes from the Clar to the Kekulé type of pattern as the width of the ribbon increases. All of the values in the upper part of the graph coincide with Kekulé structures (shadowed in gray in Figure 7), whereas the values below correspond to the Clar-patterned GNRs (also shadowed). It is clear, however, that, despite the width or type of arrangement at the edges, Kekulé-patterned GNRs always present higher values for the band gap. This is due to the localization of electrons in the structure. Electrons in Kekulé structures are more localized, which makes these ribbons less polarizable, showing a higher band gap. On the contrary, the electronic delocalization in Clar structures is higher, and the band gap smaller, as will also be seen in the transport property calculations (vide infra). This is in contrast to the nonfunctionalized zigzag GNRs (in red in Figure 7), where the band gap is almost zero in all cases (semimetallic behavior) and the delocalization is the highest. The fact that the electronic delocalization and, therefore, the aromaticity is so closely related to the transport properties of GNRs is of major importance, because it shows how rational edge functionalization creates aromaticity patterns and opens the band gap of these otherwise-semimetallic materials.

Taking into account that a band gap of around 1 eV is desirable for electronic applications, similarly ot common semiconductor materials, the graph of Figure 7 becomes an interesting tool for

dx.doi.org/10.1021/jp410032h | J. Phys. Chem. C 2013, 117, 26371–26384

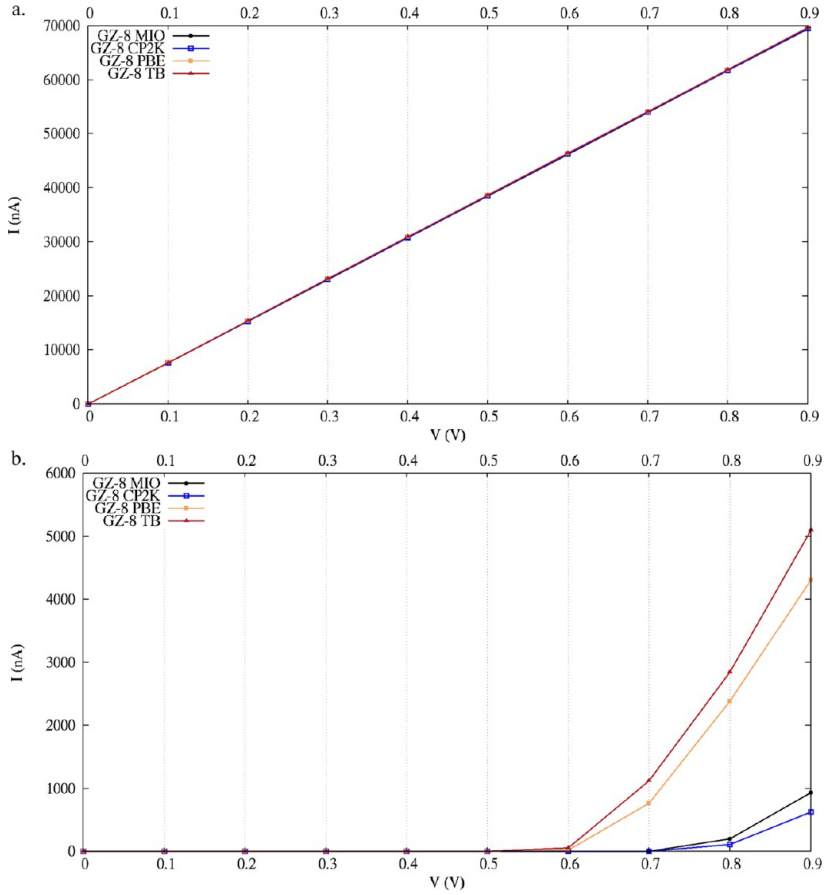

Figure 11. $I-V$ characteristics at 300 K of pristine (a) GZ-8 and (b) GZ-8 O a2 using various methods.

estimating the width and tailored edge needed to reach this value. Obviously, more accurate calculations on the exact band-gap values of GNRs could improve this map, but that fact does not diminish the qualitative importance of this study. With the values provided here, according to Figure 7, if our zigzag GNR is less than approximately 15 Å in width, a Clar aromaticity pattern is desirable, and therefore, the appropriate tailored edge should be designed for that purpose. On the other hand, if a width over 20 Å is reached, a Kekulé pattern results in a band gap closer to 1 eV, and a different tailored edge should be designed accordingly to create this aromaticity pattern. Actually, GZ-10 and GZ-11 GNRs, which present widths close to 25 Å, are the structures with the closest band-gap value to 1 eV. When the width is between 15 and 20 Å, both Kekulé and Clar structures are equally possible. Kekulé-patterned GNRs have gaps slightly greater than 1 eV, whereas for Clar structures, the band gap is less than 1 eV. If any value other than 1 eV is needed, the combination of width and edge should be selected following these ideas. Although this discussion is just for the AH functionalization, the same reasoning is equally applicable to the O and CD functionalizations.

Induced Aromaticity Patterns on Zigzag CNTs. Furthermore, the similarity between CNTs and GNRs pointed out by Martín-Martínez et al. in a study of the electronic confinement and aromaticity of armchair GNRs[16] brings up the question of whether the edges of finite zigzag CNTs can also be rationally tailored to induce aromaticity patterns. Nevertheless, in this case, only those zigzag CNTs with $(3n,0)$ indices can be functionalized with a one-of-three type of functionalization; otherwise, the functionalized positions do not coincide when completing a lap around the edge. Figure 8 shows finite fragments of a (12,0) CNT with lengths equivalent to the widths of GZ-8 and GZ-9 GNRs.

It is clearly noticed that the patterns appear when the edge of the CNT is tailored. This fact evidences once more the equal confinement of electrons in finite CNTs and GNRs. The aromaticity patterns observed for CNTs are equivalent to the patterns described in Figure 5 for GNRs.

The (12,0) CNT with $N_z = 8$ (in length) presents a Clar-type aromaticity pattern when the a1 arrangement is set but a Kekulé pattern when the arrangement is a2. This happens again for all types of functionalization (AH, O, and CD). In the case of a (12,0) CNT with $N_z = 9$, the c1 arrangement induces a Kekulé aromaticity pattern, whereas the c2 arrangement induces a Clar-type pattern.

Clar's Sextet Theory Analysis. The presence of these patterns can be understood using Clar's sextet theory. According to Clar's theory, the configurations with the highest numbers of Clar rings along the structure will combine to provide the final aromaticity distribution. In the case of GNRs, there are three possible arrangements of Clar rings, depending on the position in which the first Clar ring is placed. Figure 9 shows the unit cell for a GZ-8 GNR functionalized with AH. In Figure 9a, the a1 arrangement for the AH functionalization is shown. There are no unpaired electrons at the edges, as is the case for nonfunctionalized zigzag GNRs (Figure 2), although the three different configurations are affected differently when additional hydrogen atoms are added. In fact, in two of these configurations, these additional hydrogen atoms coincide with the location of Clar sextets (red circles in Figure 9). Therefore, it is not possible to place a circle in these positions, because this

dx.doi.org/10.1021/jp410032h | J. Phys. Chem. C 2013, 117, 26371−26384

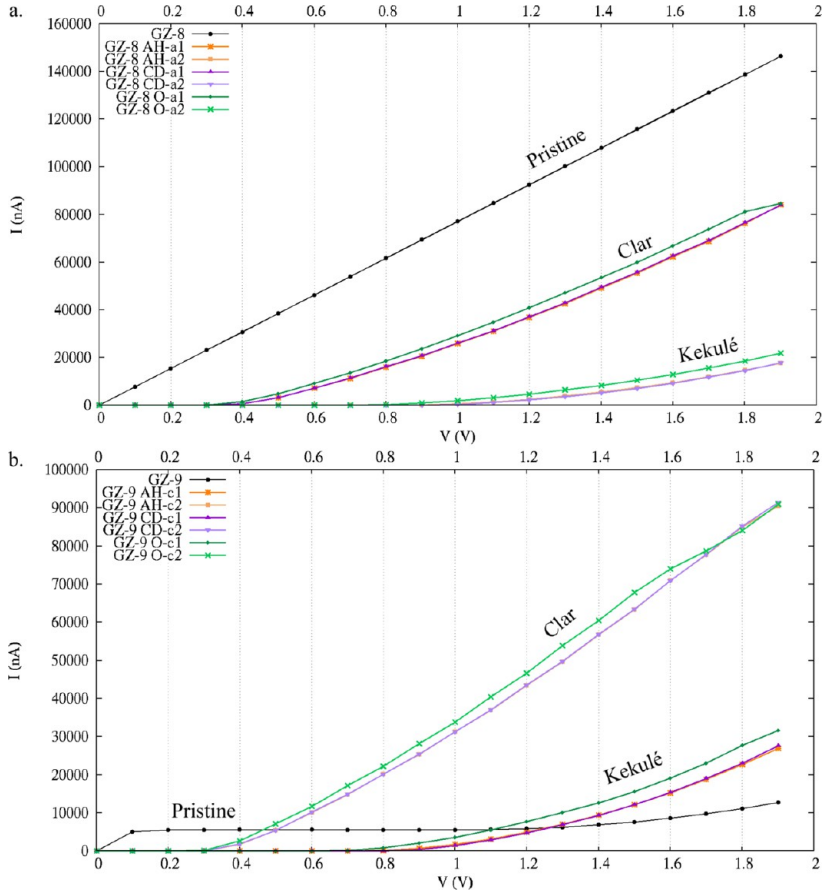

Figure 12. *I*−*V* characteristics at 300 K of all of the investigated (a) GZ-8 and (b) GZ-9 GNRs using DFTB in conjunction with the MIO parameter set.

ring is no longer aromatic, and these configurations are penalized. Because of this penalization, the Clar configuration is able to present not eight Clar rings, but seven. Therefore, this configuration contributes less to the final structure. In contrast, the configuration on the left side of Figure 9a remains unaffected because the functionalization coincides with rings that do not contain Clar sextets, and consequently, this configuration is not penalized by the functionalization. The result is that the three configurations do not have the same number of Clar rings, as happened before (see Figure 2), but only one of the three presents the maximum number of Clar rings (highlighted in a dashed green box). Now, the final structure corresponds mainly to the already described Clar pattern, shown in a green box in the right part of Figure 9a.

When the functionalization is done in an a2 arrangement at the edges of the GZ-8 GNR (Figure 9b), the situation changes slightly. Now, only one of the three configurations is penalized (the one with red circles on the left side of Figure 9b), and therefor, e the combination of the two remaining configurations (unaffected by the functionalization) gives a Kekulé-patterned structure (see the green box on the right side of Figure 9b). It is important to note that, whereas the penalized configurations go from eight to seven Clar rings in the a1 arrangement (Figure 9a), in the case of the a2 arrangement, the penalized configuration goes from eight to six Clar rings. The latter is therefore double penalized, because two Clar rings are erased from the structure, and this fact further decreases its contribution to the final structure. This explains why Kekulé patterns are more pronounced. In the case of Clar patterns, the contributions of the penalized configurations still remain to a certain degree, because only one Clar ring is erased. Conversely, in the case of Kekulé patterns, the double penalization almost deletes this configuration from contributing to the final structure.

In the case of a GZ-9 GNR the situation is similar. As shown in Figure 10, now, the c1 arrangement leads to a Kekulé pattern (Figure 10a), whereas the c2 arrangement leads to a Clar pattern (Figure 10b). The reasoning is equal to that for the GZ-8 GNR. Also, the Kekulé pattern is more pronounced in this ribbon, and again, this is due to the double penalization in the case of this pattern, whereas in the case of the Clar pattern, the configurations are single penalized.

Calculations of Transport Properties. To study the changes in conductivity when aromaticity patterns are induced and the band gap is opened by edge functionalization, the transport properties were calculated for both GZ-8 and GZ-9 GNRs.

For benchmarking, we calculated the transport properties using different methods on the pristine and functionalized GZ-8 GNR. From Figure 11, it is clear that the shape of the *I*−*V* curves (which are dependent on the DOS and the transmission spectrum) is virtually independent of the applied method. However, in the case of semiconductor-type GNRs, the current turn-up, which depends mainly on the band gap, occurs at slightly different voltages. This difference falls within the achievable accuracy of the applied methods, and the different methods give practically the same results. However, the fact that the *I*−*V* curves are independent of the applied methods is valid only for GNRs with hydrogens and oxygens at the edges and cannot necessarily be extended to other, nongraphitic systems.

dx.doi.org/10.1021/jp410032h | J. Phys. Chem. C 2013, 117, 26371−26384

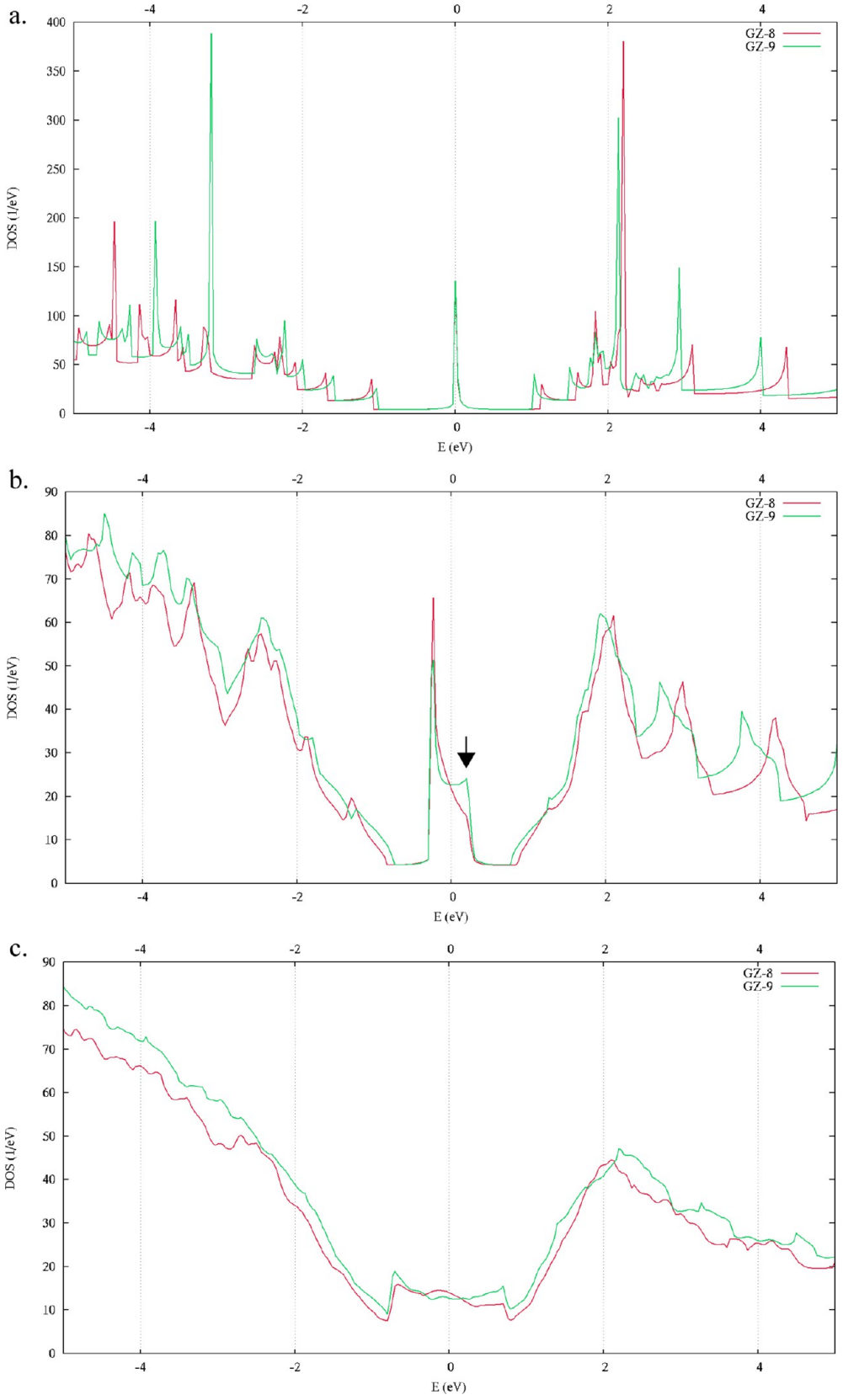

Figure 13. Densities of states of GZ-8 and GZ-9 GNRs at (a) 0, (b) 0.5, and (c) 1.5 V using the PBE/DZ level of theory. The Fermi level of the device is shifted to E = 0 eV.

Figure 12 shows the $I-V$ curves for all of the different configurations of the GZ-8 and GZ-9 GNRs under study. It can be seen that GZ-8 is a metallic conductor, having a linear $I-V$ curve. On the other hand, GZ-9, because of its symmetry, behaves as expected, despite its zero band gap: At low bias, it is an insulator, and at high bias, it is a conductor.[56] The low current at low biases

dx.doi.org/10.1021/jp410032h | J. Phys. Chem. C 2013, 117, 26371−26384

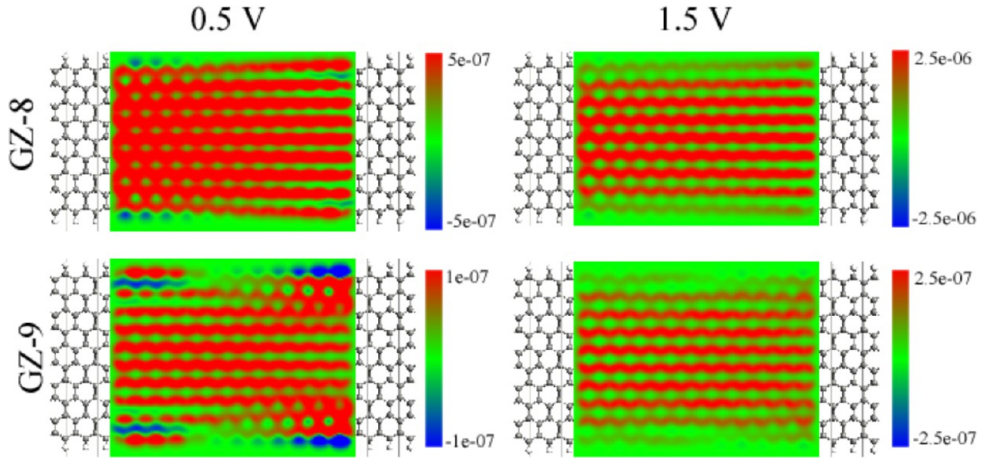

Figure 14. Current densities (in A Bohr^{-3}) at 300 K 1.0 Å above the nanoribbon plane using the PBE/DZ level of theory.

at 300 K is a consequence of the (thermal) Fermi broadening of the holes and electrons; this means that GZ-9 would be a semiconductor at 0 K. All functionalized GZ-8 and GZ-9 GNRs (AH, CD, and O functionalizations) behave like semiconductors, having their transitions from insulators to conductors according to their band gaps. Systems with a Clar-type aromaticity pattern start conducting at a lower bias than systems with a Kekulé-type pattern, as expected from the values of their band gaps. This allows the ad hoc design of semiconductors based on zigzag GNRs with different "on voltages", as needed for a desired application.

We also investigated the $I-V$ characteristics of GZ-6, GZ-7, GZ-10, and GZ-11 GNRs. We found that the $I-V$ characteristics of GZ-6, GZ-8, and GZ-10 are metallic and that GZ-7, GZ-9, and GZ-11 are similar to each other, the only difference being that the metallic regimes of the $I-V$ curves start at consistently lower voltages. The origin of this $I-V$ curve shape can be explained by symmetry.[56] Breaking the symmetry using different edge functionalizations makes GZ-9 more conducting. The DOS is rather similar in the case of GZ-8 and GZ-9 at 0 V bias (Figure 13a). However, there is a significant difference at 0.5 V (Figure 13b), marked with an arrow, which is a consequence of the coupling between the π and π^* states.[56] Note that the DOS is higher in the high-energy region (between the chemical potential of the two electrodes) in the GZ-9 ribbon, as $\pi-\pi^*$ hopping is symmetry-forbidden. As a consequence, unoccupied orbitals remain unstabilized as the electron hopping from the valence band is forbidden. At higher bias voltages, when both GNRs are conducting, there is less difference between the DOS (Figure 13c).

Finally, we also investigated the current density of GZ-8 and GZ-9 GNRs, to depict the spatial distribution of the conducting channels. The current density maps gives us information about how the electron flux is spatially distributed in the different GNRs. Because the spatial distribution is not uniform, one can conclude that the electrons are flowing in conducting channels. (Figure 14).

As expected, in the plane of the ribbon, the current density is zero (not shown in the figure), because only the π electrons and orbitals, which having a nodal plane in the plane of the GNR, are contributing to the electron transport. This means that the conducting channels are constructed only from the carbon p_z orbitals. The current density patterns are practically independent of the distance from which they are calculated from, that is, the distance above or below the plane of the GNR. However, the absolute values are rather different. One canclearly identify the two different patterns in the current density at low bias voltages (0.5 V). In the case of the GZ-8 GNR, the current is mainly flowing in the same direction. In contrast, there are serious backward current flows (in blue) in the GZ-9 GNR, making a kind of self-induced barrier for electronic transport. In other words, there are large ring currents in GZ-9 GNR and other GNRs with odd widths. Note that the currents flowing perpendicular to the transport direction cannot be seen, because only the component of the current in the transport direction was calculated. It is also worth mentioning that, at low voltage insignificant ring currents are present around the edge Hydrogens in GZ-8 GNR. In higher biases the ring currents are disappearing in both GZ-9 and GZ-9 GNRs, making the current flow strictly in the transport direction (in red). It is a well-known fact that the empty and occupied orbitals that are closer to the Fermi level are more localized on the edges, so the conduction is taking place mainly in the central region of the GNRs at higher biases and is not limited to the edge region, showing that wide range of orbitals are involved in the electronic transport at room temperature.

CONCLUSIONS

Cutting graphene into one-dimensional GNRs is one of the most suitable ways for opening band gaps in this two-dimensional material. Nevertheless, this electronic confinement in one direction is very sensitive to the width, edge shape, and edge functionalization of these very narrow strips of graphene. In particular, among highly symmetric types of GNRs, only armchair-edged ribbons are expected to present energy band gaps that are useful for electronic applications, whereas zigzag structures remain semimetallic, with a band gap close to zero.

The band gap of GNRs, and, in particular, the semimetallic behavior of zigzag structures is very closely connected to the aromaticity distribution along these materials. Therefore, understanding the fundamental reasons for the different aromaticity distributions provides a useful way to rationally design the aromaticity patterns and consequently control the band gap of GNRs.

Therefore, based on the basic concepts of Clar's sextet theory, which explains why zigzag GNRs present uniform geometries, we performed a rational design of the edges of these ribbons, inducing aromaticity patterns and opening the band gap. In this way, additional hydrogen, oxygen, and carbon deletion edge

dx.doi.org/10.1021/jp410032h | J. Phys. Chem. C 2013, 117, 26371−26384

functionalizations are shown to be equivalent ways to induce either Clar or Kekulé aromaticity patterns on GNRs. The band-gap opening as a consequence of these patterns is closely dependent on the kind of pattern, and the Kekulé-patterned ribbons present the highest band gap.

This edge functionalization also applies to zigzag CNTs and the same patterns are induced by a similar edge design. This fact points out, once more, the similar electronic confinement on GNRs and CNTs.

Finally, calculations support the band-gap-opening predictions based on aromaticity studies, and these results, together with the aromaticity analysis and the Clar's sextet theory rationalization, provide a robust design of zigzag GNR's edges toward real electronic applications.

These findings open the path to the rational design of semiconductors from zigzag GNRs with a specific bang gap and on voltage, based on the desired application.

AUTHOR INFORMATION

Corresponding Author

*E-mail: fjmartinmartinez@gmail.com.

Notes

The authors declare no competing financial interest.

ACKNOWLEDGMENTS

The authors acknowledge support from the Research Foundation Flanders (FWO); the Free University of Brussels through Grant GOA77; and the COST Materials, Physical and Nanosciences (MPNS) Action MP0901: "Designing Novel Materials for Nanodevices—From Theory to Practice (NanoTP)".

REFERENCES

(1) Geim, A. K.; Novoselov, K. S. The Rise of Graphene. *Nat. Mater.* **2007**, *6*, 183−191.
(2) Novoselov, K. S.; Geim, A. K.; Morozov, S. V.; Jiang, D.; Katsnelson, M. I.; Grigorieva, I. V.; Dubonos, S. V.; Firsov, A. A. Two-Dimensional Gas of Massless Dirac Fermions in Graphene. *Nature* **2005**, *438*, 197−200.
(3) Meyer, J. C.; Geim, A. K.; Katsnelson, M. I.; Novoselov, K. S.; Booth, T. J.; Roth, S. The Structure of Suspended Graphene Sheets. *Nature* **2007**, *446*, 60−63.
(4) Han, M. Y.; Özyilmaz, B.; Zhang, Y.; Kim, P. Energy Band-Gap Engineering of Graphene Nanoribbons. *Phys. Rev. Lett.* **2007**, *98*, 206805.
(5) Barone, V.; Hod, O.; Scuseria, G. E. Electronic Structure and Stability of Semiconducting Graphene Nanoribbons. *Nano Lett.* **2006**, *6*, 2748−2754.
(6) Iijima, S. Helical Microtubules of Graphitic Carbon. *Nature* **1991**, *354*, 56−58.
(7) Cai, J.; Ruffieux, P.; Jaafar, R.; Bieri, M.; Braun, T.; Blankenburg, S.; Muoth, M.; Seitsonen, A. P.; Saleh, M.; Feng, X.; Müllen, K.; Fasel, R. Atomically Precise Bottom-up Fabrication of Graphene Nanoribbons. *Nature* **2010**, *466*, 470−473.
(8) Blankenburg, S.; Cai, J.; Ruffieux, P.; Jaafar, R.; Passerone, D.; Feng, X.; Müllen, K.; Fasel, R.; Pignedoli, C. A. Intraribbon Heterojunction Formation in Ultranarrow Graphene Nanoribbons. *ACS Nano* **2012**, *6*, 2020−2025.
(9) Li, X.; Wang, X.; Zhang, L.; Lee, S.; Dai, H. Chemically Derived, Ultrasmooth Graphene Nanoribbon Semiconductors. *Science* **2008**, *319*, 1229−1232.
(10) Berger, C.; Song, Z.; Li, X.; Wu, X.; Brown, N.; Naud, C.; Mayou, D.; Li, T.; Hass, J.; Marchenkov, A. N.; Conrad, E. H.; First, P. N.; de Heer, W. A. Electronic Confinement and Coherence in Patterned Epitaxial Graphene. *Science* **2006**, *312*, 1191−1196.
(11) Chen, Z.; Lin, Y.-M.; Rooks, M. J.; Avouris, P. Graphene Nano-Ribbon Electronics. *Physica E* **2007**, *40*, 228−232.
(12) Koskinen, P.; Malola, S.; Häkkinen, H. Self-Passivating Edge Reconstructions of Graphene. *Phys. Rev. Lett.* **2008**, *101*, 115502.
(13) Kusakabe, K.; Maruyama, M. Magnetic Nanographite. *Phys. Rev. B* **2003**, *67*, 092406.
(14) Yamashiro, A.; Shimoi, Y.; Harigaya, K.; Wakabayashi, K. Spin- and Charge-Polarized States in Nanographene Ribbons with Zigzag Edges. *Phys. Rev. B* **2003**, *68*, 193410.
(15) Son, Y.-W.; Cohen, M. L.; Louie, S. G. Energy Gaps in Graphene Nanoribbons. *Phys. Rev. Lett.* **2006**, *97*, 216803.
(16) Wagner, P.; Ivanovskaya, V. V.; Melle-Franco, M.; Humbert, B.; Adjizian, J.-J.; Briddon, P. R.; Ewels, C. P. Ripple Edge Engineering of Graphene Nanoribbons. *Phys. Rev. B* **2013**, *88*, 094106.
(17) Wagner, P.; Ivanovskaya, V. V.; Rayson, M. J.; Briddon, P. R.; Ewels, C. P. Mechanical Properties of Nanosheets and Nanotubes Investigated Using a New Geometry Independent Volume Definition. *Condens. Matter* **2013**, *25*, 155302.
(18) Martín-Martínez, F. J.; Fias, S.; Van Lier, G.; De Proft, F.; Geerlings, P. Electronic Structure and Aromaticity of Graphene Nanoribbons. *Chem.—Eur. J.* **2012**, *18*, 6183−6194.
(19) Wassmann, T.; Seitsonen, A. P.; Saitta, A. M.; Lazzeri, M.; Mauri, F. Structure, Stability, Edge States, and Aromaticity of Graphene Ribbons. *Phys. Rev. Lett.* **2008**, *101*, 096402.
(20) Martín-Martínez, F. J.; Fias, S.; Van Lier, G.; De Proft, F.; Geerlings, P. Tuning Aromaticity Patterns and Electronic Properties of Armchair Graphene Nanoribbons with Chemical Edge Functionalisation. *Phys. Chem. Chem. Phys.* **2013**, *15*, 12637−12647.
(21) Matsuo, Y.; Tahara, K.; Nakamura, E. Theoretical Studies on Structures and Aromaticity of Finite-Length Armchair Carbon Nanotubes. *Org. Lett.* **2003**, *5*, 3181−3184.
(22) Baldoni, M.; Sgamellotti, A.; Mercuri, F. Electronic Properties and Stability of Graphene Nanoribbons: An Interpretation Based on Clar Sextet Theory. *Chem. Phys. Lett.* **2008**, *464*, 202−207.
(23) Selli, D.; Baldoni, M.; Sgamellotti, A.; Mercuri, F. Redox-Switchable Devices Based on Functionalized Graphene Nanoribbons. *Nanoscale* **2012**, *4*, 1350−1354.
(24) Clar, E. *The Aromatic Sextet*; Wiley: London, 1972.
(25) Solà, M. Forty Years of Clar's Aromatic π-Sextet Rule. *Front. Chem.* **2013**, 1.
(26) Baldoni, M.; Sgamellotti, A.; Mercuri, F. Finite-Length Models of Carbon Nanotubes Based on Clar Sextet Theory. *Org. Lett.* **2007**, *9*, 4267−4270.
(27) Baldoni, M.; Selli, D.; Sgamellotti, A.; Mercuri, F. Unraveling the Reactivity of Semiconducting Chiral Carbon Nanotubes through Finite-Length Models Based on Clar Sextet Theory. *J. Phys. Chem. C* **2008**, *113*, 862−866.
(28) Wassmann, T.; Seitsonen, A. P.; Saitta, A. M.; Lazzeri, M.; Mauri, F. Clar's Theory, π-Electron Distribution, and Geometry of Graphene Nanoribbons. *J. Am. Chem. Soc.* **2010**, *132*, 3440−3451.
(29) Fujii, S.; Enoki, T. Clar's Aromatic Sextet and π-Electron Distribution in Nanographene. *Angew. Chem., Int. Ed.* **2012**, *51*, 7236−7241.
(30) Martín-Martínez, F. J.; Melchor, S.; Dobado, J. A. Edge Effects, Electronic Arrangement, and Aromaticity Patterns on Finite-Length Carbon Nanotubes. *Phys. Chem. Chem. Phys.* **2011**, *13*, 12844−12857.
(31) Van Lier, G.; Fowler, P. W.; De Proft, F.; Geerlings, P. A Pentagon Proximity Model for local Aromaticity in Fullerenes and Nanotubes. *J. Phys. Chem. A* **2002**, *106*, 5128−5135.
(32) Frisch, M. J.; Trucks, G. W.; Schlegel, H. B.; Scuseria, G. E.; Robb, M. A.; Cheeseman, J. R.; Scalmani, G.; Barone, V.; Mennucci, B.; Petersson, G. A.; Nakatsuji, H.; Caricato, M.; Li, X.; Hratchian, H. P.; Izmaylov, A. F.; Bloino, J.; Zheng, G.; Sonnenberg, J. L.; Hada, M.; Ehara, M.; Toyota, K.; Fukuda, R.; Hasegawa, J.; Ishida, M.; Nakajima, T.; Honda, Y.; Kitao, O.; Nakai, H.; Vreven, T.; Montgomery, J. A., Jr.; Peralta, J. E.; Ogliaro, F.; Bearpark, M.; Heyd, J. J.; Brothers, E.; Kudin, K. N.; Staroverov, V. N.; Keith, T.; Kobayashi, R.; Normand, J.; Raghavachari, K.; Rendell, A.; Burant, J. C.; Iyengar, S. S.; Tomasi, J.; Cossi, M.; Rega, N.; Millam, J. M.; Klene, M.; Knox, J. E.; Cross, J. B.;

Bakken, V.; Adamo, C.; Jaramillo, J.; Gomperts, R.; Stratmann, R. E.; Yazyev, O.; Austin, A. J.; Cammi, R.; Pomelli, C.; Ochterski, J. W.; Martin, R. L.; Morokuma, K.; Zakrzewski, V. G.; Voth, G. A.; Salvador, P.; Dannenberg, J. J.; Dapprich, S.; Daniels, A. D.; Farkas, Ö.; Foresman, J. B.; Ortiz, J. V.; Cioslowski, J.; Fox, D. J. *Gaussian 09*, revision A.1; Gaussian, Inc.: Wallingford, CT, 2009.
(33) Heyd, J.; Scuseria, G. E.; Ernzerhof, M. Hybrid Functionals Based on a Screened Coulomb Potential. *J. Chem. Phys.* **2003**, *118*, 8207; **2006**, *124*, 219906.
(34) Barone, V.; Hod, O.; Peralta, J. E.; Scuseria, G. E. Accurate Prediction of the Electronic Properties of Low-Dimensional Graphene Derivatives Using a Screened Hybrid Density Functional. *Acc. Chem. Res.* **2011**, *44*, 269−279.
(35) Plasser, F.; Pašalić, H.; Gerzabek, M. H.; Libisch, F.; Reiter, R.; Burgdörfer, J.; Müller, T.; Shepard, R.; Lischka, H. The Multiradical Character of One- and Two-Dimensional Graphene Nanoribbons. *Angew. Chem., Int. Ed.* **2013**, *52*, 2581−2584.
(36) Costa Girão, E.; Liang, L.; Cruz-Silva, E.; Filho, A. G. S.; Meunier, V. Emergence of Atypical Properties in Assembled Graphene Nanoribbons. *Phys. Rev. Lett.* **2011**, *107*, 135501.
(37) Deleuze, M. S.; Huzak, M.; Hajgató, B. Half-Metallicity of Graphene Nanoribbons and Related Systems: A New Quantum Mechanical El Dorado for Nanotechnologies ... or a Hype for Materials Scientists? *J. Mol. Model.* **2013**, *19*, 2699−2714.
(38) Huzak, M.; Deleuze, M. S.; Hajgató, B. Half-Metallicity and Spin-Contamination of the Electronic Ground State of Graphene Nanoribbons and Related Systems: An Impossible Compromise? *J. Chem. Phys.* **2011**, *135*, 104704.
(39) Hajgató, B.; Deleuze, M. S. Quenching of Magnetism in Hexagonal Graphene Nanoflakes by Non-Local Electron Correlation. *Chem. Phys. Lett.* **2012**, *553*, 6−10.
(40) Hajgató, B.; Szieberth, D.; Geerlings, P.; De Proft, F.; Deleuze, M. S. A Benchmark Theoretical Study of the Electronic Ground State and of the Singlet−Triplet Split of Benzene and Linear Acenes. *J. Chem. Phys.* **2009**, *131*, 224321.
(41) Hajgató, B.; Huzak, M.; Deleuze, M. S. Focal Point Analysis of the Singlet−Triplet Energy Gap of Octacene and Larger Acenes. *J. Phys. Chem. A* **2011**, *115*, 9282−9293.
(42) Poater, J.; Bofill, J. M.; Alemany, P.; Solà, M. Local Aromaticity of the Lowest-Lying Singlet States of [*n*]Acenes (*n* = 6−9). *J. Phys. Chem. A* **2005**, *109*, 10629−10632.
(43) TubeAnalyzer. Software developed by S. Melchor, Grupo de Modelización y Diseño Molecular, Universidad de Granada, Granada, Spain, 2007.
(44) Bultinck, P.; Ponec, R.; Van Damme, S. Multicenter Bond Indices as a New Measure of Aromaticity in Polycyclic Aromatic Hydrocarbons. *J. Phys. Org. Chem.* **2005**, *18*, 706−718.
(45) Martín-Martínez, F. J.; Melchor, S.; Dobado, J. A. Clar−Kekulé Structuring in Armchair Carbon Nanotubes. *Org. Lett.* **2008**, *10*, 1991−1994.
(46) Brandbyge, M.; Mozos, J.-L.; Ordejón, P.; Taylor, J.; Stokbro, K. Density-Functional Method for Nonequilibrium Electron Transport. *Phys. Rev. B* **2002**, *65*, 165401−165418.
(47) Elstner, M.; Porezag, D.; Jungnickel, G.; Elsner, J.; Haugk, M.; Frauenheim, T.; Suhai, S.; Seifert, G. Self-Consistent-Charge Density-Functional Tight-Binding Method for Simulations of Complex Materials Properties. *Phys. Rev. B* **1998**, *58*, 7260−7268.
(48) Stokbro, K.; Petersen, D. E.; Smidstrup, S.; Blom, A.; Ipsen, M.; Kaasbjerg, K. Semiempirical Model for Nanoscale Device Simulations. *Phys. Rev. B* **2010**, *82*, 075420.
(49) *Atomistix ToolKit*, version 12.8.2; QuantumWise A/S: Copenhagen, Denmark; www.quantumwise.com, 2012.
(50) Brandbyge, M.; Mozos, J.-L.; Ordejón, P.; Taylor, J.; Stokbro, K. Density-Functional Method for Nonequilibrium Electron Transport. *Phys. Rev. B* **2002**, *65*, 165401.
(51) Soler, J. M.; Artacho, E.; Gale, J. D.; García, A.; Junquera, J.; Ordejón, P.; Sánchez-Portal, D. The SIESTA Method for *ab Initio* Order-*N* Materials Simulation. *J. Phys.: Condens. Matter* **2002**, *14*, 2745.
(52) Perdew, J. P.; Burke, K.; Ernzerhof, M. Generalized Gradient Approximation Made Simple. *Phys. Rev. Lett.* **1996**, *77*, 3865−3868.
(53) Cerdá, J.; Soria, F. Accurate and Transferable Extended Hückel-Type Tight-Binding Parameters. *Phys. Rev. B* **2000**, *61*, 7965−7971.
(54) About CP2K. http://www.cp2k.org/, 2013.
(55) Monkhorst, H. J.; Pack, J. D. Special Points for Brillouin-Zone Integrations. *Phys. Rev. B* **1976**, *13*, 5188−5192.
(56) Li, Z.; Qian, H.; Wu, J.; Gu, B.-L.; Duan, W. Role of Symmetry in the Transport Properties of Graphene Nanoribbons under Bias. *Phys. Rev. Lett.* **2008**, *100*, 206802.